Dual-Band Resistance Compression Networks for Improved Rectifier Performance

Kyriaki Niotaki, *Student Member, IEEE*, Apostolos Georgiadis, *Senior Member, IEEE,* Ana Collado, *Senior Member, IEEE*, and John S. Vardakas, *Member, IEEE*.

***Abstract*— In this work, the concept of dual-band resistance compression networks is introduced and applied to the design of rectifier circuits with improved performance. The use of resistance compression networks (RCNs) minimizes the sensitivity of rectifier circuits to variations in the surrounding environment, such as input power level and changes in the rectifier load. The proposed dual-band RCN can be used as the matching network located between the antenna and the rectifying element of a dual-band rectifier for energy harvesting applications. A dual-band (915 MHz / 2.45 GHz) rectifier based on RCN is designed and characterized showing improved performance in comparison with a conventional dual-band envelope detector by exhibiting improved RF-dc conversion efficiency and reduced sensitivity versus output load and input power variations.**

***Index Terms*—dual-band rectifier, energy harvesting, resistance compression network, wireless power transfer.**

I. Introduction

RF energy harvesting and wireless power transfer are receiving special attention due to the increasing need for autonomous devices to implement concepts such as the Internet of Things (IoT), machine-to-machine communications, and the Internet of Everything (IoE) [1]. In this context the design of efficient and self-sustained devices is of key importance and the use of energy harvesting solutions has been investigated to achieve this autonomy [2]. Among the different types of energy harvesting solutions, electromagnetic energy harvesting, where the energy from existing electromagnetic signals in the environment is collected and transformed to dc power, has received a lot of attention [3].

Rectenna elements collect RF signals and transform them to dc power using a certain rectifying element, such as Schottky diodes [4],[5]. Since ambient electromagnetic energy is available in low levels, the design of efficient energy harvesters that can harvest simultaneously the ambient energy from different frequency bands is desirable to achieve enough harvested dc power. Multi-band and broadband rectenna circuits have already been proposed in the literature [6]-[13].

Electromagnetic energy harvesters are usually optimized for specific operating conditions, including frequency of operation, input power level and fixed output load. However, the available electromagnetic energy is not a constant value and depends on the surrounding environment conditions, such as the propagation environment. A variation in the available input power level at the rectenna results in a variation of the input impedance of the nonlinear rectifying device and thus a deviation from the nominal operating conditions. This causes degradation of the rectifier performance due to the impedance mismatch and thus, the harvested power level is reduced.

The output of the rectenna is usually connected to a varying load, such as dc-dc converter or regulator circuit. The load variation due to the time varying operating conditions of the circuitry also results in an input impedance change in the rectifying device and thus, in degraded performance. According to [14], maximum RF-dc conversion efficiency is achieved for a specific selection of output resistance value, while the optimum load varies versus frequency.

In order to reduce the sensitivity of the rectifier circuits versus load and input power variations, novel circuits have been recently proposed in the literature [15] namely resistance compression networks (RCNs). These networks achieve small variations in the input impedance of the rectifier circuit under large variations of input power levels and output load values.

Various implementations of resistance compression networks have been presented in the literature depending on the application scenario and the operating frequency. RCNs have been implemented using lumped element components and transmission line implementations [15]-[20]. These networks have been successfully applied for the design of dc-dc converters, harmonically terminated rectifiers and outphasing energy recovery amplifier systems [15]-[20].

So far, resistance compression networks operating at a single frequency have been proposed in the literature. Here we propose the design of a dual-band resistance compression network based rectifier with reduced sensitivity to input impedance and output load variations. The design of multi-band and/or broadband resistance compression networks is of great importance for plenty of applications, including energy harvesting and power electronic circuits. The design of multiband and broadband rectennas with reduced sensitivity to the surrounding environment conditions is an even more challenging task for increasing the harvested power level in energy harvesters.

Manuscript received July 01, 2014. This paper is an expanded version from the IEEE MTT-S International Microwave Symposium, Tampa Bay, FL, USA, June 1-6 2014. This work was supported by the Spanish Ministry of Economy and Competitiveness and FEDER funds through the project TEC2012-39143. This work was also supported by the COST Action IC1301 Wireless Power Transmission for Sustainable Electronics (WIPE) and by the Generalitat de Catalunya under grant 2014 SGR 1551.

K. Niotaki, A. Georgiadis and A. Collado are with the Centre Tecnologic de Telecomunicacions de Catalunya (CTTC), Castelldefels, 08860, Spain (e-mail: kniotaki@cttc.es).

J.S. Vardakas is with Iquadrat, Barcelona, Spain (e-mail: jvardakas@iquadrat.com).

The concept of dual-band resistance compression networks based rectifiers has been introduced in [21], where preliminary results of this work have been presented. In this work, two RCN topologies are introduced and their behavior is presented in detail. An analytical equation about the input impedance of the rectifying device is mathematically derived to show the dependence of the input impedance of the diode to the input RF amplitude and output dc voltage. A performance comparison between two rectifier topologies based on different RCNs is made, where it is shown that improved performance is achieved by cascading two unit cells at each branch of the RCN based rectifier. A detailed analysis of the rectifier design is also presented with an adequate set of measurements showing that the proposed rectifier shows a good RF-dc conversion efficiency with minimized sensitivity to input power and load variations.

The outline of this work is as follows. In Section II, the properties of the dual-band resistance compression networks are described. Section III presents some design considerations for the design of the proposed topology along with the performance evaluation of the RCN based rectifier in comparison with a conventional envelope detector rectifier. In Section IV, the fabricated 915 MHz/2.45 GHz RCN based rectifier experimental results are presented showing reduced sensitivity to input power and load variations. Finally, the conclusions of the proposed work are presented.

II. Dual-Band Resistance Compression Network (RCN) Theory

A resistance compression network is a matching network that reduces the sensitivity of electronic circuits, such as rectifiers, to variations in the input power level and in the output load. In this Section, the operating principles of the dual-band resistance compression networks are presented.

The basic structure of a resistance compression network consists of two branches that exhibit opposite phase response of the input impedance (φ and $-\varphi$ respectively) at the operating frequency (f) as Fig. 1a illustrates. In this topology, the input impedance of the network (Z_{in}) suffers small variations under large variations of the real load values.

Taking into account the operating principles of an RCN, dual-band and in general multi-band RCN should similarly exhibit opposite phase response at an arbitrary set of frequencies, as Fig. 1b depicts for the dual-band case. A way to achieve the necessary phase conditions can be the use of unit circuit cells consisting of series and shunt LC network (Fig. 2a) [22]. The unit cell shown in this figure can be used as a dual-band matching network operating at an arbitrary set of frequencies (f_1 and f_2). In particular, at the low operating frequency (f_1), the discrete elements C_R and L_R tend to be open and short, respectively. In the same way, C_L and L_L tend to be short and open at the high operating frequency (f_2).

The unit cell shown in Fig. 2a exhibits a negative phase response ($-\varphi_1$) at the low operating frequency (f_1) and a positive phase response (φ_2) at the higher frequency (f_2). A simple manner to obtain the opposite phase response in the two branches is to use the same unit network but mirror it by reversing the input and output ports (Fig. 2b). The unit cell of Fig. 2b shows opposite phase response at the two selected frequencies if compared to the unit cell in Fig. 2a: φ_1 at the low frequency f_1 and $-\varphi_2$ at the high frequency f_2. A dual-band resistance compression effect can be achieved by placing the conventional and reversed unit cells into the two branches of the RCN, as Fig. 3 depicts (topology RCN1).

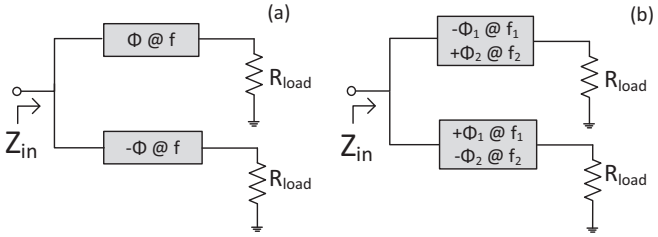

Fig. 1. a) Resistance compression networks operating at a single frequency. Each branch exhibits opposite phase response (φ and $-\varphi$) at the operating frequency (f) and b) Dual-band RCNs. Each branch exhibits opposite phase response at the two operating frequencies (f_1 and f_2).

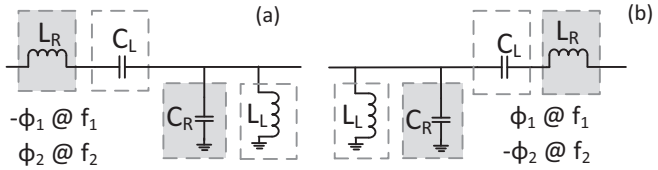

Fig. 2. a) Unit circuit cell consisting of a series and shunt LC network and b) Rearranged circuit cell (the same network as Fig. 2a with reversed input and output ports).

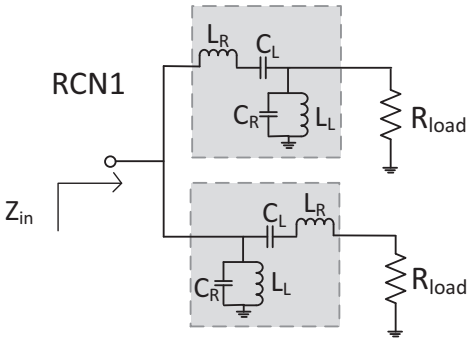

Fig. 3. Dual-band resistance compression network implemented with a single circuit cell at each branch. The proposed topology is indicated as RCN1.

As it has been previously described, dual-band resistance compression can be achieved by using a single unit cell at each branch of the resistance compression network topology (RCN1 in Fig. 3). A resistance compression can also be achieved by cascading identical unit cells at each branch of the network, as shown in Fig. 4. The structure of Fig. 4 will be referred to as RCN2. Such a structure offers more degrees of freedom in defining the resistance compression properties.

The input impedance (Z_{in}) of the networks shown in Fig. 3 and Fig. 4 can be derived by using the equivalent model in Fig. 5b of the unit cell of Fig. 5a, where the series elements are represented by an impedance Z and the parallel elements by an admittance Y. Then, the dual-band RCN of the topology RCN1 (Fig. 3) can be represented as a combination of impedances and admittances as Fig. 5a illustrates. The same applies for the topology of RCN2 (Fig. 4). The impedance and admittance of a unit cell are given by (1) and (2), respectively [22].

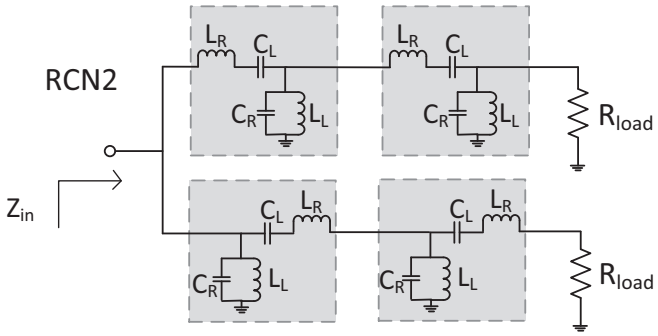

Fig. 4. Dual-band resistance compression network. The proposed topology (with two unit cells at each branch of the network) is indicated as RCN2.

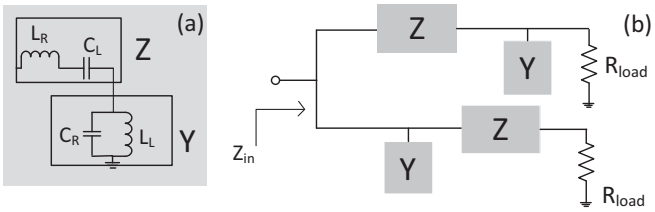

Fig. 5. a) Equivalent network for an ideal unit cell represented as a set of complex impedance (Z) and admittance (Y) and b) Equivalent network of the dual–band RCN (RCN1) in terms of complex impedances.

$$Z = j\left(\omega L_R - \frac{1}{\omega C_L}\right) \quad (1)$$

$$Y = j\left(\omega C_R - \frac{1}{\omega L_L}\right) \quad (2)$$

Straightforward calculations result in the estimation of the input impedance of such networks. For instance, the Z_{in} of the RCN1 topology is given by (3) as a combination of Z, Y and R_{load}.

$$Z_{in} = \left((R_{load} + Z)(R_{load} + Z + R_{load}ZY)\right) / \left((R_{load}{}^2ZY^2 + 2R_{load}{}^2Y + R_{load}Z^2Y^2 + 4R_{load}ZY + 2R_{load} + Z^2Y + 2Z)\right) \quad (3)$$

In order to demonstrate the properties of the proposed topologies (RCN1 and RCN2) two networks have been designed to have dual-band operation at 915 MHz and 2.45 GHz. The compression ratio of the input impedance is defined as the ratio between the largest and smallest values of $|Z_{in}|$ and is compared with the ratio between the largest and smallest values of the corresponding R_{load} variations, as it is shown in Fig. 6 and Fig. 7.

The compression behavior of the topologies RCN1 and RCN2 are depicted in Fig. 6 and Fig. 7, respectively. The magnitude of the input impedance of the networks ($|Z_{in}|$) is plotted versus the output load (R_{load}) for both operating frequencies. Fig. 6 and Fig. 7 also show the percentage of the delivered power from the 50 Ω source to the input of the rectifier circuit showing explicitly how the matching is affected for each R_{load} value. The values of the elements used to obtain the compression characteristics of the RCN topologies are shown in Table I.

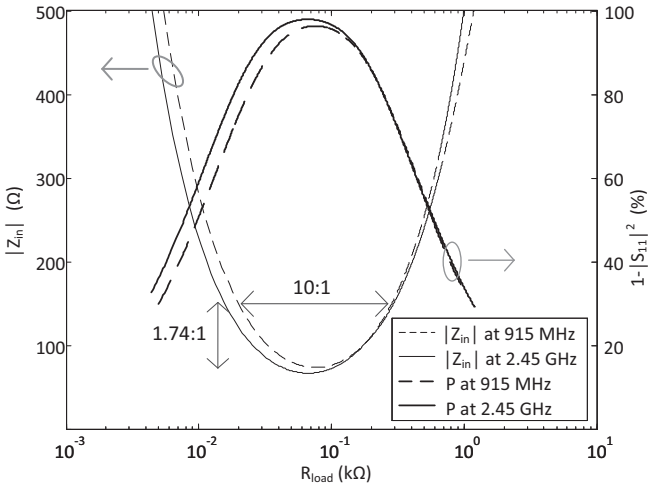

Fig. 6. Magnitude of the input impedance ($|Z_{in}|$) and percentage of the delivered power to the input of the rectifier for the RCN1 topology (Fig. 3) versus load variations (R_{load}).

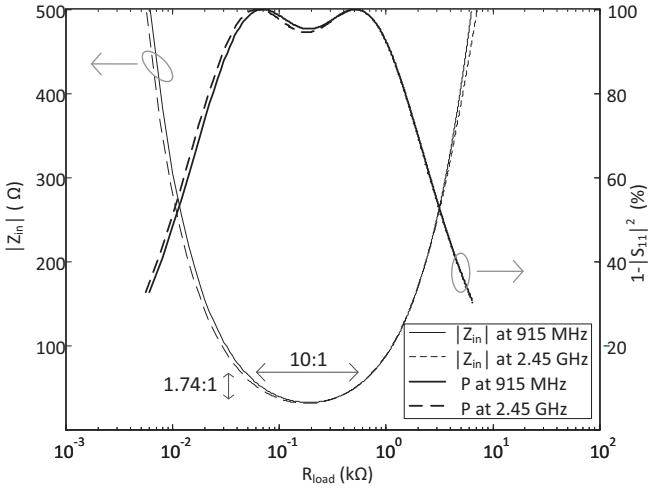

Fig. 7. Magnitude of the input impedance ($|Z_{in}|$) and percentage of the delivered power to the input of the rectifier for the RCN2 topology (Fig. 4) versus load variations (R_{load}).

TABLE I
COMPONENT VALUES USED TO OBTAIN THE DATA AT FIG. 6 AND FIG. 7

Component Values for RCN1 topology (Fig. 3)		Component Values for RCN2 topology (Fig. 4)	
L_R	7.15 nH	L_R	5.55 nH
C_R	3 pF	C_R	1.14 pF
L_L	4 nH	L_L	10.15 nH
C_L	1.5 pF	C_L	2 pF

The compression of the RCN1 topology (Fig. 3) is shown in Fig. 6. For an R_{load} range from 24.2 Ω to 242 Ω (a ratio of 10:1 around the central compression point), the $|Z_{in}|$ varies from 73 Ω to 127 Ω (a ratio of 1.74:1) at 915 MHz. In the same way, a 10:1 variation of R_{load} (from 21.2 Ω to 212 Ω) results in 1.74:1 variation of $|Z_{in}|$ (66.7 Ω to 116 Ω) at 2.45 GHz. Thus, the same compression ratio is achieved for both frequencies around the center compression point.

The compression characteristics of the RCN2 topology are shown in Fig. 7. The center value of the compression curve of RCN2 at 915 MHz (2.45 GHz) corresponds to the values of R_{load}=189 Ω and $|Z_{in}|$=32.2 Ω (R_{load}=179 Ω and $|Z_{in}|$=31 Ω). A 10:1 variation of R_{load} values (from 60 Ω to 600 Ω) is

compressed to 1.74:1 ratio (from 32.2 Ω to 56 Ω) at $|Z_{in}|$ at 915 MHz. Finally, the same compression ratios are achieved for a variation of R_{load} from 57 Ω to 570 Ω (a ratio of 1:10) to the compressed variation of $|Z_{in}|$ from 31 Ω to 54 Ω (1:1.74) at 2.45 GHz.

III. Dual-Band RCN based Rectifier

A. Design considerations for the dual-band RCN based rectifier topology

In rectifier circuits, output load and input power level variations result in an impedance change at the input of the diode. This impedance variations result in an impedance mismatch between the antenna and the rectifying element and thus, in degraded performance. Therefore, resistance compression network topologies have been considered, such as the ones in the previous Section, to be used in the design of rectifier circuits.

Here, the dual-band resistance compression networks are placed as the matching network located between the input of a Schottky diode and an antenna represented by a 50 Ω source. Fig. 8a and Fig. 8b show the RCN1 and RCN2 topologies presented in the previous Section when applied for the design of a dual-band rectifier.

One can see that in the proposed implementations of the RCN based rectifier (Fig. 8a and Fig. 8b) there is only one output load if compared with the traditional implementations of RCN where two separate loads are used for each of the branches (Fig. 3 and Fig. 4). However it has to be considered that in the RCN based rectifier topologies, the loads of the RCN are the Schottky diodes of the rectifier. The capacitances that are placed at the output of the rectifier isolate the two branches at RF frequencies which lead to a similar structure to the one in Fig. 3 and Fig. 4 where the loads are the complex input impedances of the diodes (Z_1).

The electrical behavior of the diodes can be expressed as complex impedance (Z_1). The formula for the calculation of Z_1 derives from the analysis of the electrical behavior of the proposed structures (Fig. 8a and Fig. 8b). Let us assume a sinusoidal input signal equal to v_1=Ecos(ωt), where E is the amplitude and ω the frequency of the input signal (Fig. 9a). The current through the diodes D1 and D2 as a function of the voltage across the terminals of the diodes are given by (4) and (5), respectively,

$$i_1 = I_{s1}\left(e^{\frac{v_1 - V_L}{V_t}} - 1\right) \quad (4)$$

$$i_2 = I_{s2}\left(e^{\frac{-V_L}{V_t}} - 1\right) \quad (5)$$

where V_t is the thermal voltage and V_L (V_L=$I_L R_L$) is the output dc voltage of the circuit, assuming that C_{out} is ideal and provides a perfect RF short at the output of the diodes.

At RF frequencies the two branches of the proposed structure are isolated because of the dc capacitor at the output of the network. Considering only the behavior of a single diode at RF (Fig. 9b), the diode current (i_1) can be calculated (taking into account the voltage drop across the diode that is equal to Ecos(ωt)-V_L) as

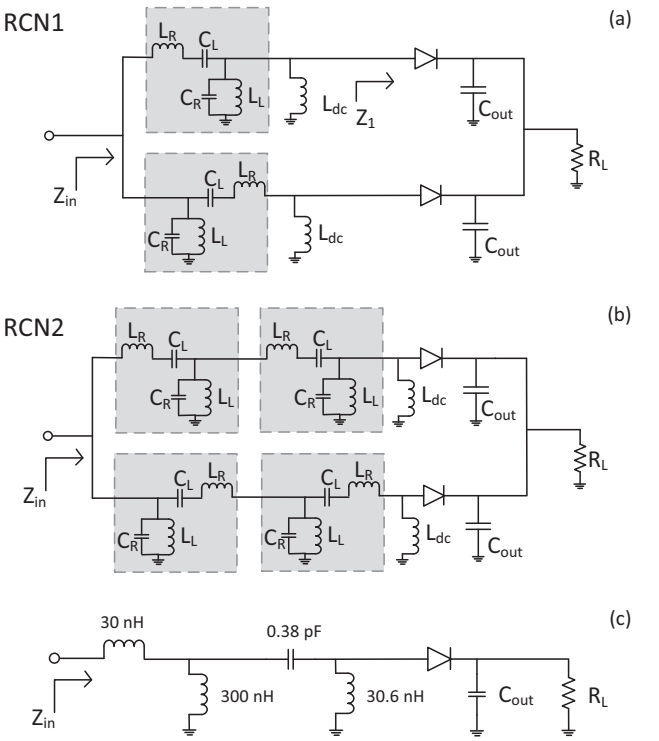

Fig. 8. Schematics of the simulated dual-band rectifiers: a) proposed RCN based rectifier with RCN1 topology, b) proposed RCN based rectifier with RCN2 topology and c) conventional envelope detector topology.

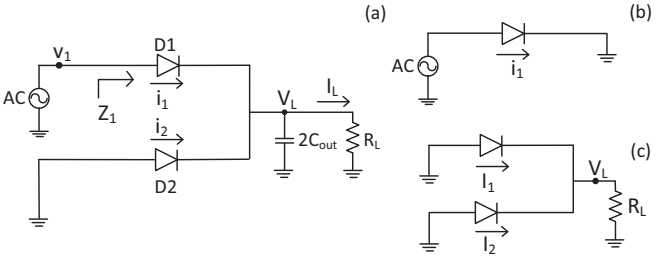

Fig. 9. a) Simplified circuit topology of the proposed rectifier topology, b) equivalent circuit of the diode (D1) at RF and c) dc equivalent circuit of the proposed structure.

$$i_1 = I_{s1}\left(e^{\frac{E\cos(\omega t) - V_L}{V_t}} - 1\right) \quad (6)$$

Taking into account the modified Bessel function series expansion, similarly to [23] and shown in (7), the current through the diode (i_1) can be expressed as in (8) and then approximated by the sum of only the dc and the first harmonic contributions as in (9).

$$e^{x\cos\omega t} = B_o(x) + 2\sum_{n=1}^{\infty} B_n(x)\cos(n\omega t) \quad (7)$$

$$i_1 = I_{s1}\left(e^{\frac{-V_L}{V_t}} B_0\left(\frac{E}{V_t}\right) - 1\right) + 2I_{s1}e^{\frac{-V_L}{V_t}}\sum_{n=1}^{\infty} B_n\left(\frac{E}{V_t}\right)\cos n\omega t \quad (8)$$

$$i_1 \cong I_1 + 2I_{s1}e^{\frac{-V_L}{V_t}} B_1\left(\frac{E}{V_t}\right)\cos\omega t \quad (9)$$

with

$$I_1 = I_{s1}\left(e^{\frac{-V_L}{V_t}} B_0\left(\frac{E}{V_t}\right) - 1\right) \quad (10)$$

Note that the two branches of the proposed topologies (Fig. 8a and Fig. 8b) are dc coupled which affects the diode impedance. The dc equivalent circuit of the structure is shown in Fig. 9c. At the dc analysis, the output dc current is given by

$$I_1 + I_2 = I_L \quad (11)$$

The output dc voltage (V_L) can be calculated by substituting (10) into (11). The result, shown in (12), demonstrates that V_L depends on the amplitude of the input signal E (and therefore the input power) and the output resistance (R_L).

$$I_{s1}\left(e^{-\frac{V_L}{Vt}} B_0\left(\frac{E}{V_t}\right) - 1\right) + I_{s2}\left(e^{-\frac{V_L}{Vt}} - 1\right) = \frac{V_L}{R_L} \quad (12)$$

The RF resistance of the diode can be calculated by dividing the RF voltage difference across the diode terminals v_1 with the RF current flowing into the diode from (9) which gives

$$Z_1 = \frac{E}{2I_{s1} e^{-\frac{V_L}{Vt}} B_1\left(\frac{E}{V_t}\right)} \quad (13)$$

From (12) and (13), one can see that the input impedance of the diode (Z_1) depends both on the input voltage (through the amplitude E) and the output load R_L (through V_L). Considering that $V_L=I_L R_L$, the input impedance of the diode is also given by (14).

$$Z_1 = \frac{E}{2I_{s1} e^{-\frac{I_L R_L}{Vt}} B_1\left(\frac{E}{V_t}\right)} \quad (14)$$

B. Design of the dual band RCN based rectifier

One of the most widely used metrics for the evaluation of the performance of rectifiers is the RF-dc conversion efficiency (15), which is calculated as the fraction of the harvested dc power (P_{DC}) and the RF available power (P_{RF}) [24].

$$\eta = \frac{P_{DC}}{P_{RF}} \quad (15)$$

The maximum RF-dc conversion efficiency of rectifier circuits is achieved for a specific selection of output load that varies with the frequency [14]. The design of broadband and multi-band rectifier circuits implies that a compromise of the performance among the operating frequencies should be made.

A RCN based dual-band rectifier is designed to operate at f_1=915 MHz and f_2=2.45 GHz. The RCN2 topology is selected for this design, as simulation (Fig. 10) has shown that the rectifier achieved improved performance with the RCN2 (Fig. 8b) topology in comparison with the RCN1 topology (Fig. 8a). Fig. 10a and Fig. 10b show the performance of the rectifier versus input power level and output load, where better results are achieved using two unit cells.

In order to be able to evaluate the performance of the proposed RCN based rectifier, a dual-band rectifier based on an envelope detector topology is also designed and optimized for maximum efficiency at 915 MHz and 2.45 GHz. The design and optimization of the two rectifiers is made using a commercial simulator (Agilent ADS). A harmonic balance (HB) analysis is used along with Large Signal Scattering Parameter (LSSP) analysis for the optimization of the circuits [24]-[27]. Optimization goals are used to impose constraints on both the minimum RF-dc conversion efficiency of the circuit and the input impedance matching (Z_{in}) at f_1 and f_2. The selected rectifying device is a low threshold Schottky diode (SMS7630) from Skyworks.

The schematic of the conventional single diode envelope detector is shown in Fig. 8c, while the proposed RCN based rectifier is depicted in Fig. 8b. The values of the unit cells are chosen in such a way that the total phase difference for each branch has opposite sign at both operating frequencies. An additional inductor (L_{dc}=100 nH) is also placed as a dc path to the ground at the input of the diode (Fig. 8b).

A performance comparison of the proposed RCN based rectifier and the envelope detector is presented in Fig. 11 - Fig. 14. Their performance is evaluated in terms of the simulated RF-dc conversion efficiency versus R_L for an input power level of 0 dBm at the low operating frequency (Fig. 11) and at the high operating frequency (Fig.12). One can see that there is a larger range of output loads (R_L) for which the RF-dc conversion efficiency remains above 50% for the case of the RCN based rectifier if compared to the envelope detector.

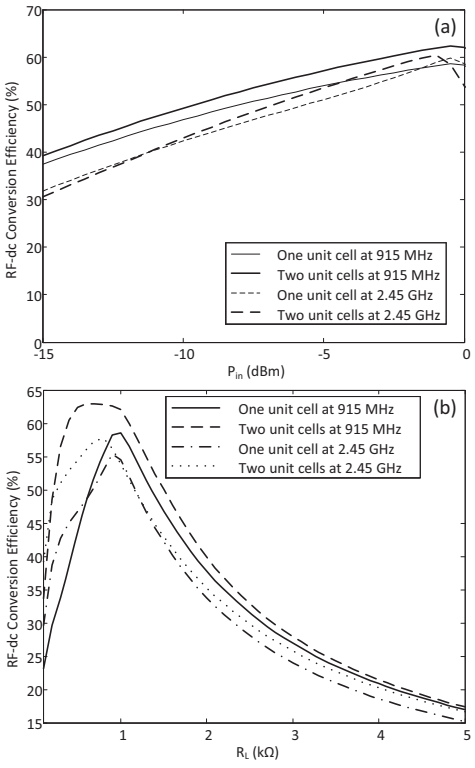

Fig. 10. Performance comparison of a RCN based rectifier with a single (RCN1 topology) and two unit cells at each branch of the RCN (RCN2 topology): a) versus input power (for R_L=1 kΩ) and b) output load (for P_{in}=0 dBm).

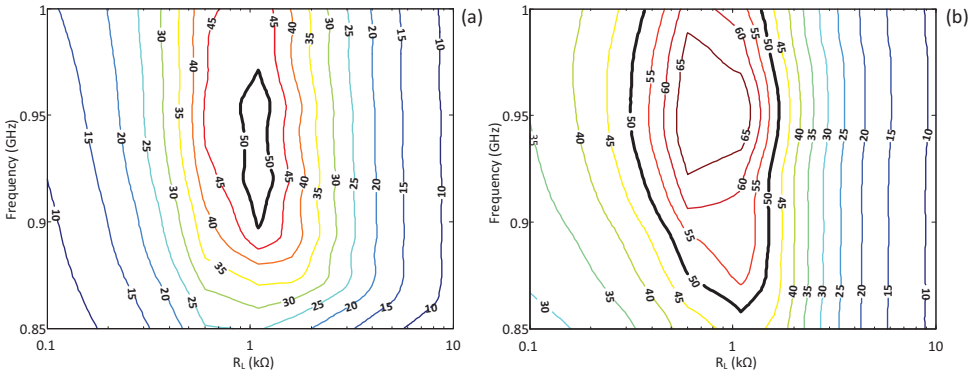

Fig. 11. RF-dc conversion efficiency (%) of a) the envelope detector rectifier and b) the RCN based rectifier for an input power of 0 dBm at the 915 MHz band.

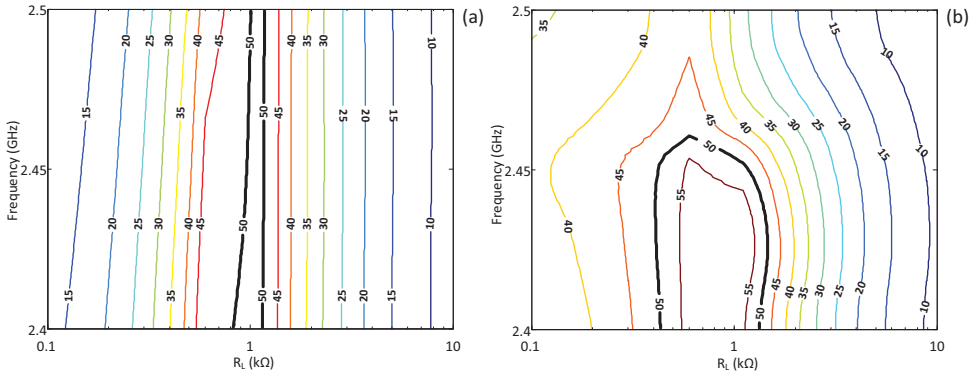

Fig. 12. RF-dc conversion efficiency (%) of a) the envelope detector rectifier and b) the RCN based rectifier for an input power of 0 dBm at the 2.45 GHz band.

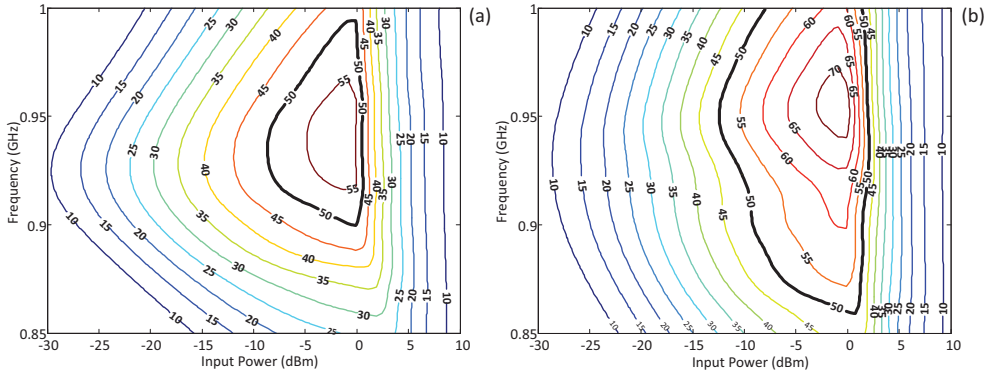

Fig. 13. RF-dc conversion efficiency (%) of a) the envelope detector rectifier and b) the RCN based rectifier for R_L=1 kΩ at the 915 MHz band.

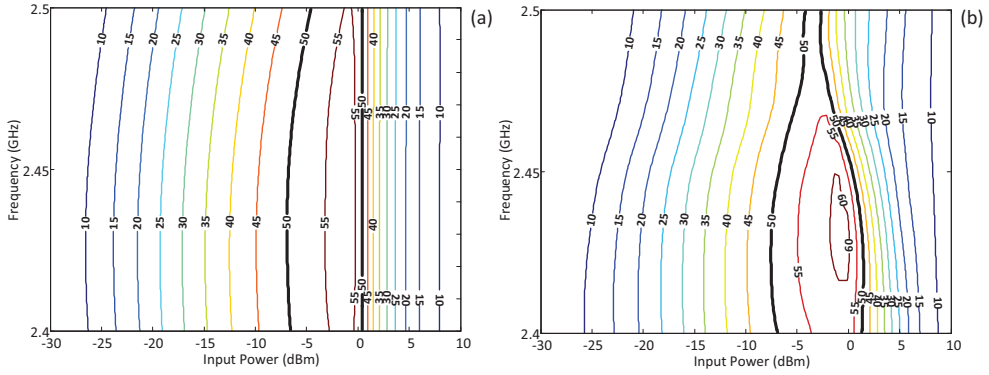

Fig. 14. RF-dc conversion efficiency (%) of a) the envelope detector rectifier and b) the RCN based rectifier for R_L=1 kΩ at the 2.45 GHz band.

The RF-dc conversion efficiency versus input power level for a selected output load (R_L=1 kΩ) for both operating frequencies is also presented in Fig. 13 and Fig. 14. It can be observed that the RF-dc conversion efficiency of the proposed RCN based rectifier remains higher than 50% for a larger range of input power levels in comparison with the envelope detector rectifier. In conclusion, as it can be seen from Fig. 11-Fig. 14, the proposed RCN based rectifier is less sensitive to input power and output load variations than the conventional envelope detector rectifier. Additionally the RCN rectifier shows improved performance in terms of RF-dc conversion efficiency.

The RF-dc conversion efficiency for both circuits at the two operating frequencies is also shown in Fig. 15. One can see that the RCN based rectifier presents a flatter and higher value of RF-dc conversion efficiency versus the load resistance (Fig. 15a for P_{in}=0 dBm). The RF-dc conversion efficiency also maintains higher values versus input power levels. The improvement in the rectifier performance is more noticeable in certain load values (Fig. 15b for R_L= 0.51 kΩ) and in certain frequency values (Fig.15c for R_L=1 kΩ) where the RF-dc conversion efficiency maintains a higher value in a larger range of input power.

It should be noted that the RCN based rectifier shows little improvement for high load values and high input power levels, which is partially attributed to the low breakdown voltage of the diode that determines its operating range and thus, the performance of the circuit. After the breakdown voltage is reached, RCN is not able to have any significant effect.

C. Final design of the RCN based rectifier

In the previous Sections, the RCN based rectifier was designed using ideal lossless discrete elements. For the fabrication of the prototype, the ideal values of the lumped components had to be replaced with the models that are provided from the manufacturers. The layout of the rectifier circuit had also to be analyzed using electromagnetic (EM) simulation. A full-wave EM simulation was made for the design of the passive structure of the circuit. In order to evaluate the impact of the substrate losses and the EM analysis of the layout on the performance of the circuit, two curves with intermediate steps are included in this Section.

The RF-dc conversion efficiency of the proposed ideal rectifier (whose performance has been already analyzed in Section II) is shown in Fig. 16. One can see that the rectifier presents peak RF-dc conversion efficiency at the 915 MHz and 2.45 GHz frequency bands.

The second curve of Fig. 16 depicts how the introduction of the EM simulation affects the circuit performance. The layout of the circuit is simulated using the Agilent Momentum EM simulator and the obtained data are introduced in the circuit simulation. The capacitor C_R was implemented as a radial stub with width W=1.05 mm, length L=4.55 mm and angle 45º. By introducing these data at the simulation, an additional peak is observed close to the second frequency band. Additionally, the peak efficiency at the high operating frequency band is slightly shifted to a higher frequency.

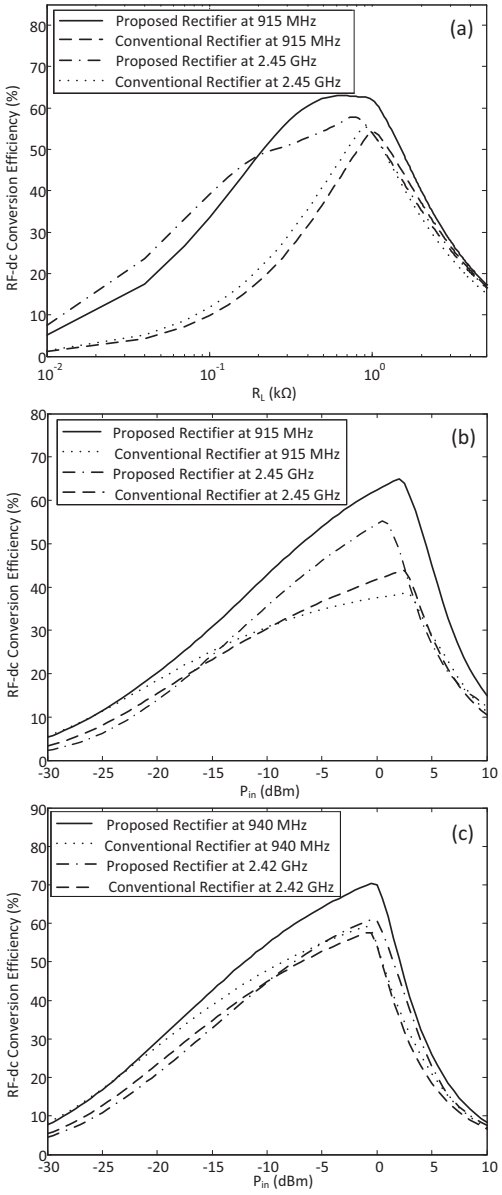

Fig. 15. Performance comparison of the conventional envelope detector topology and the proposed RCN based rectifier versus a) output load (915 MHz/2.45 GHz), b) input power level for R_L=0.51 kΩ (915 MHz/2.45 GHz), and c) input power level for R_L=1 kΩ (940 MHz/2.42 GHz).

The third curve of Fig. 16 shows the performance of the rectifier with real inductor and capacitor models but without substrate losses. So far, the obtained results show that the main source of losses of the topology is due to the discrete components losses and the layout of the circuit.

Finally, the fourth curve (solid line) shows the performance of the dual-band rectifier, including losses associated with the layout, the discrete component values and the substrate material. The rectifier has reduced efficiency at the two operating frequencies in comparison with the design of the ideal rectifier as it is expected.

The simulation resulted in the component values shown in the Table II. Commercial inductors from Coilcraft and capacitors from Murata have been used for the implementation of the rectifier. The prototype has been fabricated on Arlon

25N substrate with height of 30 mil, relative permittivity of 3.38 and loss tangent of 0.0025. The fabricated prototype is shown in Fig. 17. The measured results of the fabricated prototype are described in the next Section, where the reduced sensitivity of the dual-band RCN based rectifier to input power and output load variations is demonstrated.

TABLE II
COMPONENT VALUES FOR THE FABRICATED DUAL-BAND RCN BASED RECTIFIER

Components	Values	Components	Values
L_R	8.7 nH	C_R	0.8 pF
L_L	100 nH	C_L	27 pF
L_{dc}	100 nH	C_{out}	120 pF

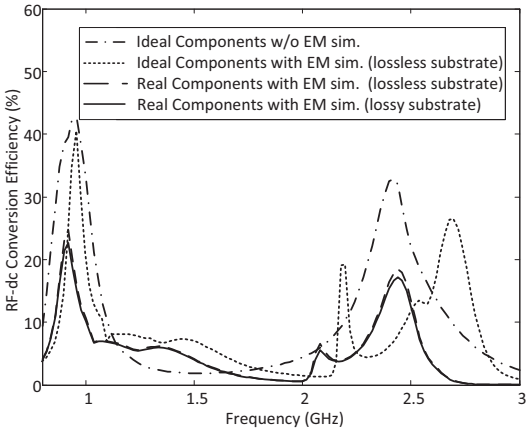

Fig. 16. Evolution of the RF-dc conversion efficiency versus operating frequency for R_L=1 kΩ and P_{in}=-15 dBm.

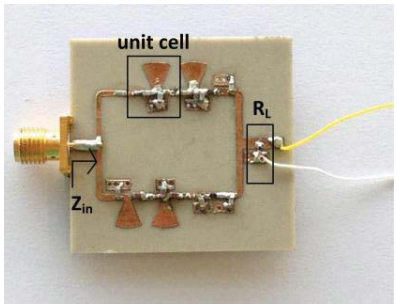

Fig. 17. Fabricated prototype of the 915 MHz/2.45 GHz RCN based rectifier.

IV. EXPERIMENTAL RESULTS

The fabricated prototype is characterized in terms of RF-dc conversion efficiency versus input power levels (P_{in}), output loads (R_L) and operating frequency. The performance of the circuit is shown in Fig. 18 - Fig. 24.

Initially, the RF-dc conversion efficiency of the circuit versus operating frequency for R_L=1 kΩ and R_L=2 kΩ is measured for P_{in}=-15 dBm (Fig. 18). One can see that the high operating frequency is slightly shifted to a higher frequency value (2.5 GHz).

A comparison between the simulated and measured reflection coefficient ($|S_{11}|$) of the RCN based rectifier for P_{in}=-15 dBm and P_{in}=0 dBm is shown in Fig. 19. The measured results show that the rectifier remains matched for a range of input power levels and that the measured results are in accordance with the simulation.

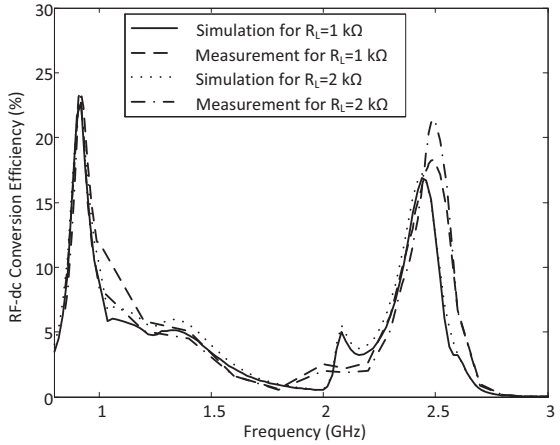

Fig. 18. Comparison of simulated and measured RF-dc conversion efficiency for an input power of -15 dBm versus operating frequency for two different load values (1 kΩ and 2 kΩ).

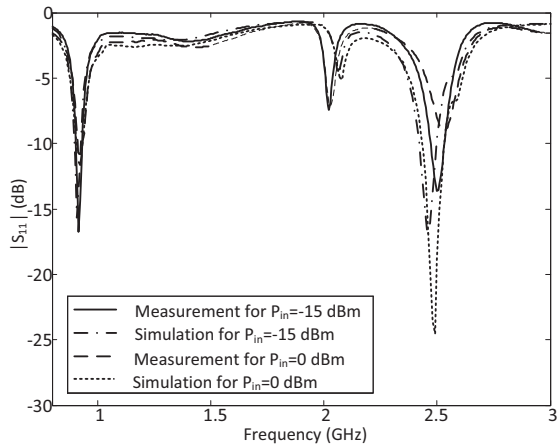

Fig. 19. Comparison of simulated and measured reflection coefficient ($|S_{11}|$) versus operating frequency for two different input power levels (-15 dBm and 0 dBm) for R_L=2 kΩ.

The measured $|S_{11}|$ versus operating frequency for R_L= 0.51 kΩ, 2 kΩ and 2.7 kΩ for a fixed P_{in} (-15 dBm) is depicted at Fig. 20. One can see from these results that the circuit also remains matched under a large variation of output loads (0.51 kΩ to 2.7 kΩ).

In order to verify the reduced sensitivity of the RCN based rectifier to input power and output load variations, a set of additional measurements has been taken (Fig. 21 to Fig. 24). The evolution of the RF-dc conversion efficiency of the proposed rectifier versus P_{in} for different load values (0.51 kΩ, 0.75 kΩ, 1 kΩ, 2 kΩ and 2.7 kΩ) at the two operating frequencies with peak RF-dc conversion efficiency (915 MHz and 2.5 GHz) is depicted at Fig. 21 and Fig. 22, respectively. As it can be observed, the evolution of the RF-dc conversion efficiency remains flat for a wide range of input power levels for R_L=0.51 kΩ, R_L=0.75 kΩ and R_L=1 kΩ. The resistance compression effect starts reducing for values greater than R_L=2 kΩ. However, the efficiency of the RCN based rectifier remains in high levels for a range of R_L and degrades smoothly.

In order to evaluate the performance of the rectifier at low input power levels, the measured RF-dc conversion efficiency

of the rectifier is plotted versus output load for low input power levels (-15 dBm, -10 dBm and -5 dBm) at 915 MHz (Fig. 23) and 2.5 GHz (Fig. 24). One can see that the efficiency remains nearly constant over a wide range of R_L for low levels of harvested power.

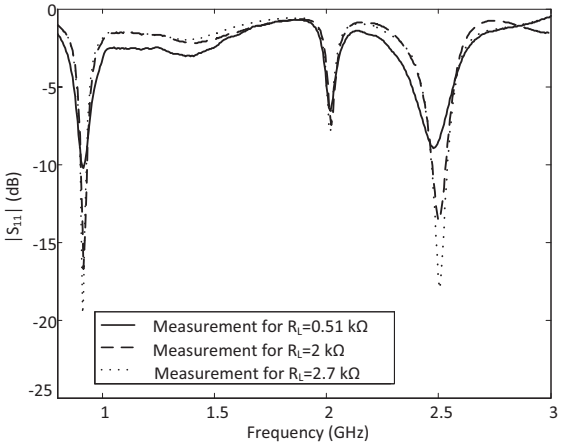

Fig. 20. Measured reflection coefficient ($|S_{11}|$) versus operating frequency for various output loads (R_L= 0.51 kΩ, 2 kΩ and 2.7 kΩ) for an input power of -15 dBm.

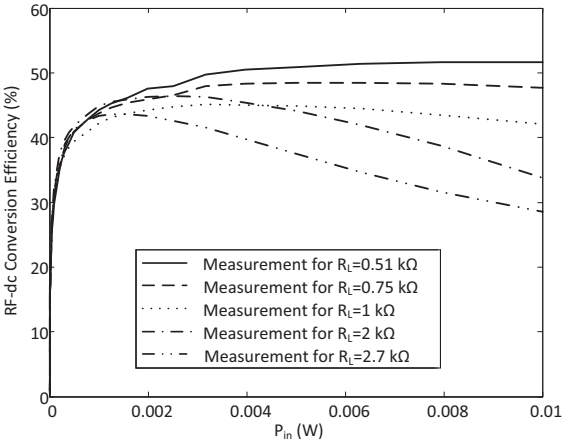

Fig. 21. Measured RF-dc conversion efficiency versus input power for various load values (0.51 kΩ, 0.75 kΩ, 1 kΩ, 2 kΩ and 2.7 kΩ) at 915 MHz.

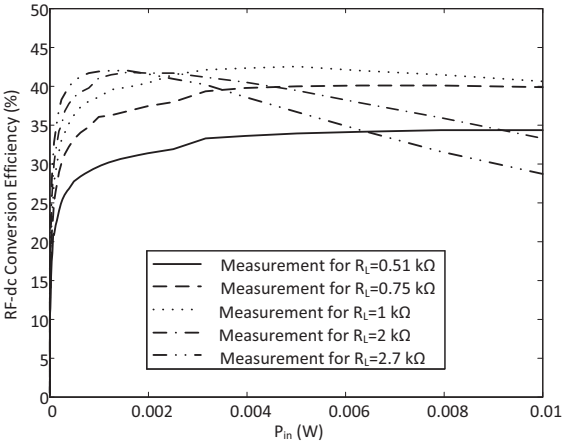

Fig. 22. Measured RF-dc conversion efficiency versus input power for various load values (0.51 kΩ, 0.75 kΩ, 1 kΩ, 2 kΩ and 2.7 kΩ) at 2.5 GHz.

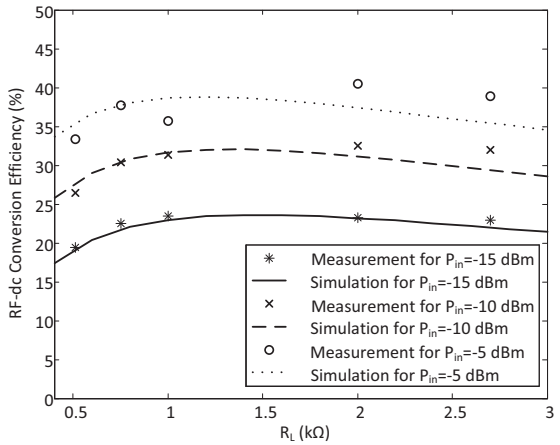

Fig. 23. Measured RF-dc conversion efficiency versus output load for a range of input power levels from -15 dBm to -5 dBm at 915 MHz.

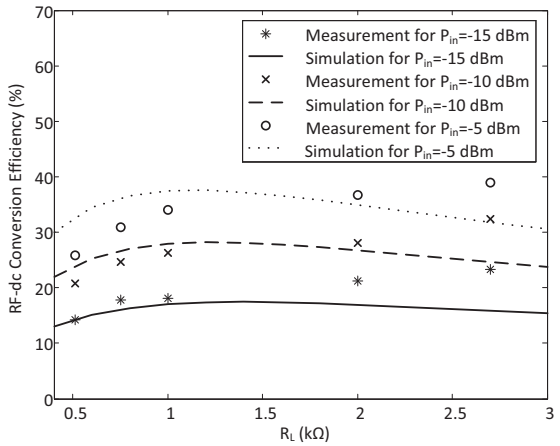

Fig. 24. Measured RF-dc conversion efficiency versus load for a range of input power levels from -15 dBm to -5 dBm at 2.5 GHz.

V. Conclusion

In this paper, dual-band resistance compression networks have been introduced and experimentally demonstrated as part of the design of a dual-band rectifier. The operation principles of these matching networks are presented in detail. Furthermore, this work presents the design of a dual-band RCN based rectifier operating at 915 MHz and 2.45 GHz. The proposed rectifier design is compared with a conventional envelope detector showing improved RF-dc conversion efficiency and reduced sensitivity to output load and input power variations.

References

[1] S. Kim, C. Mariotti, F. Alimenti, P. Mezzanotte, A. Georgiadis, A. Collado, L. Roselli and M.M. Tentzeris, "No Battery Required: Perpetual RFID-Enabled Wireless Sensors for Cognitive Intelligence Applications," *IEEE Microw. Mag.*, vol. 14, no. 5, pp. 66-77, Aug. 2013.

[2] S. Beeby and N. White, *Energy Harvesting for Autonomous Systems*, Norwood, CA: Artech House, 2010.

[3] W. C. Brown, R. H. George and N. I. Heeman, "Microwave to dc converter," U.S. Patent 3 434 678, Mar. 25, 1969.

[4] M. N. Ruíz, R. Marante and J. A. García, "A class E synchronous rectifier based on an E-pHEMT device for wireless powering applications," *in 2012 IEEE MTT-S Int. Microw. Symp. Dig.*, Montreal, QC, Canada, pp. 1–3.

[5] B. Strassner and K. Chang, "A circularly polarized rectifying antenna array for wireless microwave power transmission with over 78% efficiency," *in 2002 IEEE MTT-S Int. Microw. Symp. Dig.*, Seattle, WA, pp. 1535–1538.
[6] K. Niotaki, S. Kim, J. Seongheon, A. Collado, A. Georgiadis and M. M. Tentzeris, "A Compact Dual-Band Rectenna Using Slot-Loaded Dual Band Folded Dipole Antenna," *IEEE Antennas Wireless Propag. Lett.*, vol. 12, pp. 1634-1637, Dec. 2013.
[7] J. A. Hagerty, F. B. Helmbrecht, W. H. McCalpin, R. Zane, and Z. B. Popovic, "Recycling ambient microwave energy with broad-band rectenna arrays," *IEEE Trans. Microw. Theory Techn*., vol. 52, no. 3, pp. 1014–1024, Mar. 2004.
[8] B. L. Pham and A.V. Pham, "Triple Bands Antenna and High Efficiency Rectifier Design for RF Energy Harvesting at 900, 1900 and 2400 MHz," in *2013 IEEE MTT-S Int. Microw. Symp.*, Seattle, WA, pp.1-3.
[9] J. Heikkinen and J. M. Kivikoski, "A novel dual-frequency circularly polarized rectenna," *IEEE Antennas Wireless Propag. Lett.*, vol. 2, no. 1, pp. 330-333, Febr. 2003.
[10] Y.H. Suh, and K. Chang, "A high-efficiency dual-frequency rectenna for 2.45- and 5.8- GHz wireless power transmission," *IEEE Trans. Microw. Theory Techn.*, vol. 50, no. 7, pp. 1784–1789, Jul. 2002.
[11] A. Collado and A. Georgiadis, "Conformal Hybrid Solar and Electromagnetic (EM) Energy Harvesting Rectenna," *IEEE Trans. Circuits Syst. I, Reg. Papers*, vol. 60, no. 8, pp. 2225-2234, Aug. 2013.
[12] V. Rizzoli, G. Bichicchi, A. Costanzo, F. Donzelli, and D. Masotti, "CAD of multi-resonator rectenna for micro-power generation," *in Proc. 39th European Microw. Conf.*, Rome, Italy, 2009, pp. 1684–1687.
[13] T. Paing, J. Shin, R. Zane and Z. Popovic, "Resistor emulation approach to low-power RF energy harvesting," *IEEE Trans. Power Electron.*, vol. 23, no. 3, pp. 1494–1501, May 2008.
[14] A. Costanzo, M. Fabiani, A. Romani, D. Masotti, and V. Rizzoli, "Codesign of ultra-low power RF/microwave receivers and converters for RFID and energy harvesting applications," *in 2010 IEEE MTT-S Int. Microw. Symp. Dig.*, Anaheim, CA, pp. 856–859.
[15] Han Yehui, O. Leitermann, D.A. Jackson, J.M. Rivas and D.J. Perreault, "Resistance Compression Networks for Radio-Frequency Power Conversion," *IEEE Trans. Power Electron.*, vol. 22, no. 1, pp. 41-53, Jan. 2007.
[16] J.F. Xu, W. Tai and D.S. Ricketts, "A transmission line based resistance compression network (TRCN) for microwave applications," *in 2013 IEEE MTT-S Int. Microw. Symp. Dig*., Seattle, WA, pp. 1-3.
[17] T.W. Barton, J. Gordonson, and D.J. Perreault, "Transmission Line Resistance Compression Networks and Applications to Wireless Power Transfer," *IEEE J. Emerg. Sel. Topics Power Electron.,* Apr. 2014.
[18] W. Inam, K.K. Afridi and D.J. Perreault, "High Efficiency Resonant dc/dc Converter Utilizing a Resistance Compression Network," *IEEE Trans. Power Electron*., vol. 29, no. 8, pp. 4126-4135, Aug. 2014.
[19] P. A. Godoy, D. J. Perreault and J. L. Dawson, "Outphasing Energy Recovery Amplifier With Resistance Compression for Improved Efficiency," *IEEE Trans. Microw. Theory Techn.*, vol. 57, no. 12, pp. 2895-2906, Dec. 2009.
[20] J. Xu and D.S. Ricketts, "An Efficient, Watt-Level Microwave Rectifier Using an Impedance Compression Network (ICN) With Applications in Outphasing Energy Recovery Systems," *IEEE Microw. Compon. Lett.*, vol. 23, no. 10, pp. 542-544, Oct. 2013.
[21] K. Niotaki, A. Georgiadis and A. Collado, "Dual-Band Rectifier Based on Resistance Compression Networks," *in 2014 IEEE MTT-S Int. Microw. Symp. Dig.*, Tampa, FL, pp. 1-3.
[22] C. Caloz and T. Itoh, *Electromagnetic Metamaterials: Transmission line theory and microwave applications*, Hoboken, New Jersey: John Wiley & Sons, 2006.
[23] G. De Vita and G. Iannaccone, "Design criteria for the RF section of UHF and microwave passive RFID transponders," *IEEE Trans. Microw. Theory Techn.*, vol. 53, no. 9, pp. 2978-2990, Sept. 2005.
[24] A. Georgiadis, G. Andia-Vera, and A. Collado, "Rectenna design and optimization using reciprocity theory and harmonic balance analysis for electromagnetic (EM) energy harvesting," *IEEE Antennas Wireless Propag. Lett.*, vol. 9, pp. 444–446, May 2010.
[25] A. Boaventura, A. Collado, N.B. Carvalho, and A. Georgiadis, "Optimum behavior: Wireless power transmission system design through behavioral models and efficient synthesis techniques," *IEEE Microw. Mag.*, vol. 14, no. 2, pp. 26–35, Apr. 2013.
[26] C. R. Valenta and G. D. Durgin, "Harvesting Wireless Power: Survey of Energy-Harvester Conversion Efficiency in Far-Field, Wireless Power Transfer Systems," *IEEE Microw. Mag*., vol. 15, no. 4, pp. 108-120, Jun. 2014.
[27] K. Niotaki, S. Kim, F. Giuppi, A. Collado, A. Georgiadis and M. M. Tentzeris, "Optimized Design of Multiband and Solar Rectennas," *in Proc. IEEE Wireless Sens. Networks Top. Conf.*, Newport Beach, CA, 2014, pp. 31–33.

Kyriaki Niotaki was born in Crete, Greece. She received the B.S. in Informatics and the M.S. in Electronic Physics with specialization at Electronic Telecommunication Technology, both from Aristotle University of Thessaloniki (Greece), in 2009 and 2011, respectively. Since December 2011, she has been with the Centre Tecnologic de Telecomunicacions de Catalunya (CTTC), Barcelona, Spain, as a Research Assistant. Currently, she is working towards her Ph.D. in the Signal Theory and Communications Department of the Technical University of Catalonia (UPC), Barcelona, Spain.
Her main research interests include energy harvesting solutions and the design of power amplifiers. In 2014, she was the recipient of an IEEE Microwave Theory and Techniques Society (IEEE MTT-S) Graduate Fellowship Award.

Apostolos Georgiadis was born in Thessaloniki, Greece. He received the B.S. degree in physics and M.S. degree in telecommunications from the Aristotle University of Thessaloniki, Greece, in 1993 and 1996, respectively. He received the Ph.D. degree in electrical engineering from the University of Massachusetts at Amherst, in 2002. In 1995, he spent a semester with Radio Antenna Communications (R.A.C.), Milan Italy. In 2000, he spent three months with Telaxis Communications, South Deerfield MA. In 2002, he joined Global Communications Devices (GCD), North Andover MA, where he was a Systems Engineer involved with CMOS transceivers for wireless network applications. In June 2003, he was with Bermai Inc., Minnetonka, MN, where he was an RF/Analog Systems Architect. In 2005, he joined the University of Cantabria as a Researcher. He is currently a Senior Research Associate and Group Leader of the Microwave Systems and Nanotechnology Department at Centre Tecnològic de Telecomunicacions de Catalunya (CTTC), Barcelona, Spain, in the area of communications subsystems where he is involved in active antennas and antenna arrays and more recently with RFID technology and energy harvesting.

Dr. Georgiadis was the recipient of a 1996 Fulbright Scholarship for graduate studies with the University of Massachusetts at Amherst, the 1997 and 1998 Outstanding Teaching Assistant Award presented by the University of Massachusetts at Amherst, 1999 and 2000 Eugene M. Isenberg Award presented by the Isenberg School of Management, University of Massachusetts at Amherst, and the 2004 Juan de la Cierva Fellowship presented by the Spanish Ministry of Education and Science. He is involved in a

number of technical program committees and serves as a reviewer for several journals including IEEE Transactions on Antennas and Propagation, and IEEE Transactions on Microwave Theory and Techniques. He was the co-recipient of the EUCAP 2010 Best Student Paper Award and the ACES 2010 2nd Best Student Paper Award. He was the Chairman of COST Action IC0803, RF/Microwave communication subsystems for emerging wireless technologies (RFCSET), and the Coordinator of Marie Curie Industry-Academia Pathways and Partnerships project Symbiotic Wireless Autonomous Powered system (SWAP). He is Member of the IEEE MTT-S TC-24 RFID Technologies (Chair 2012-2014) and Member of IEEE MTT-S TC-26 Wireless Energy Transfer and Conversion. He serves at the Editorial board of the Radioengineering Journal and as an Associate Editor of the IEEE Microwave and Wireless Components Letters and IET Microwaves Antennas and Propagation Journals.

Ana Collado received the M.Sc. and Ph.D. degrees in Telecommunications Engineering from the University of Cantabria, Spain, in 2002 and 2007 respectively. She is currently a Senior Research Associate and the Project Management Coordinator at the Technological Telecommunications Center of Catalonia (CTTC), Barcelona, Spain where she performs her professional activities. Her professional interests include active antennas, substrate integrated waveguide structures, nonlinear circuit design, and energy harvesting and wireless power transmission (WPT) solutions for self-sustainable and energy efficient systems.

She has participated in several national and international research projects and has co-authored over 70 papers in journals and conferences. Among her activities she has collaborated in the organization of several international workshops in different countries of the European Union and also a Training School for PhD students. She was a Marie Curie Fellow of the FP7 project Symbiotic Wireless Autonomous Powered system (SWAP). She serves in the Editorial Board of the Radioengineering Journal and she is currently an Associate Editor of the IEEE Microwave Magazine and a member of the IEEE MTT-26 Wireless Energy Transfer and Conversion and MTT-24 RFID Technologies.

John S. Vardakas received the Dipl.-Eng. in Electrical & Computer Engineering from the Democritus University of Thrace, Greece, in 2004 and his Ph.D from the Electrical & Computer Engineering Dept., University of Patras, Greece. His research interests include teletraffic engineering, performance analysis and simulation of communication networks and especially of optical networks. He is a member of the IEEE, the Optical Society of America (OSA) and the Technical Chamber of Greece (TEE).